Registration of Dynamic MRI Data and its Impact on Diagnostic Process

Olga Kubassova[1], Roger Boyle[1], Mikael Boesen[2], Marco A. Cimmino[3], and Henning Bliddal[2]

[1] School of Computing, University of Leeds, United Kingdom,
olga@imageanalysis.org.uk, roger@comp.leeds.ac.uk
[2] The Parker Institute Frederiksberg Hospital, Frederiksberg, Denmark,
mikael.boesen@dadlnet.dkh; Henning.bliddal@frh.regionh.dk
[3] University of Genoa, Genoa, Italy, cimmino@unige.it *

Abstract. This paper discusses impact of a novel registration algorithm for dynamic MRI data on diagnosis of rheumatoid arthritis. The algorithm is based on a hybrid Euclidean-Lagrangian approach. It was applied to data acquired with low and high-field MRI scanners. The scans were processed with region-of-interest based and voxel-by-voxel approaches before and after the registration. In this paper, we demonstrate that diagnostic parameters extracted from the data before and after the registration vary dramatically, which has a crucial effect on diagnostic decision. Application of the the proposed algorithm significantly reduces artefacts incurred due to patient motion, which permits reduction of variability of the enhancement curves, yielding more distinguishable uptake, equilibrium and wash-out phases and more precise quantitative data analysis.

1 Introduction

Rheumatoid arthritis (RA) is an inflammatory disease which affects more than 0.3-1% of the adult population [1]. RA patients are often examined with Dynamic Contrast Enhanced Magnetic Resonance Imaging (DCE-MRI), where joints are imaged over time resulting in a 4D dataset. Temporal changes of signal intensity during and immediately after a bolus injection of a contrast agent reflect underlying changes in local concentration of the contrast agent, which are related to the extent of tissue inflammation. Typically, DCE-MRI data is processed on a voxel-by-voxel basis, where enhancement curves are extracted from temporal slices and evaluated using pharmacokinetic [2], heuristic [3], or region of interest (ROI) based [4] methods.

These approaches for analysis of DCE-MRI data assume that signal intensity vs. time changes at each voxel can be attributed to the contrast leakage. However, patient movement can introduce artefactual enhancement with implications to

* We thank Leeds General Infirmary, UK and The Parker Institute, DK, University of Genoa, Italy for providing data and assisting us with evaluation of the techniques.

the extracted measurements. Hands of active RA patients shiver and the range of motion is approximately 5-10mm translations and $5-15^0$ rotations in 2D and 3D planes.

Alignment of images is complicated by the non-uniformity of motion across various regions of the imaged joints and non-homogenous contract and brightness variations in later volumes.

Early registration methods [5, 6] described motion using rigid transformations that attempted to minimise the variance ratio between a pair of images. Recently, motion was modelled using optical flow and affine transformation [7, 8]. However, some optical flow techniques rely on the assumption that the contrast of the target and source images remains constant while positions of objects change, which is untrue for DCE-MRI datasets.

To align DCE-MRI data, we have modified the algorithm presented in [9], which was designed to deal with partial occlusions. We augmented the registration model with a Euclidean-Lagrangian incremental approach, which was motivated by the fact that some tissue significantly changes its intensity and brightness in the post-contrast images and therefore alignment of the post-contrast source to the pre-contrast target may not be accurate.

In this article, we will present the registration model and demonstrate its value for further quantitative analysis of dynamic data.

2 Data

A total of 37 datasets acquired from patients with low-field (0.2T, ESAOTE, Italy) and high-field (1.5T, Phillips, The Netherlands) scanners were processed. 10 high-field datasets were acquired from metacarpophalangeal joints (MCPJs) in the axial direction using T_1 weighted spoiled gradient-echo sequence; TR/TE: 14/3.8; FOV/imaging matrix: 100×200mm / 128×256, slice thickness 3mm, 6 slices. Acquisition time was 142s. 27 low-field datasets were acquired from the hand, wrist, and tendon using gradient-echo and spin-echo sequences, TR/TE: 100/16 and 60/6, imaging matrix 256×256, resulting in 3 temporal slices, 22-30 images each. Acquisition time was 300s.

3 Methods

The transformation between source $f(x, y, z, t)$ and target $f(x, y, z, t-1)$ volumes takes the following form:

$$m_{13} f(x, y, z, t-1) + m_{14} = \\ f(m_1 x + m_2 y + m_3 z + m_{10}, m_4 x + m_5 y + m_6 z + m_{11}, m_7 x + m_8 y + m_9 z + m_{12}, t),$$

where $(m_1, ..., m_9)$ represent affine and $(m_{10}, ..., m_{12})$ translation parameters; m_{13} and m_{14} are spatially varying parameters which explicitly account for contrast and brightness variations. $\boldsymbol{m} = (m_1, ..., m_{14})$ are estimated locally for each small neighbourhood, but for the sake of clarity their spatial notation is dropped.

To avoid making a decision on the optimal size of the neighbourhood, the assumption that the parameters $\boldsymbol{m}$ do not change within the neighbourhood is replaced with a smoothness assumption, which implies that physical properties in the neighbourhood of a space or within the time interval do not change abruptly.

A least square measure has been employed to deduce parameters $\boldsymbol{m}$ via cost minimisation. The error function is approximated by a 1st order Taylor series expansion and differentiated to its unknowns $\boldsymbol{m}$. The result is set to zero, and the solution takes the following form:

$$\boldsymbol{m} = \Big[\sum_{x,y,z \in \Omega} \boldsymbol{c}\, \boldsymbol{c}^{\,T} \Big]^{-1} \Big[\sum_{x,y,z \in \Omega} \boldsymbol{c}\, k \Big], \tag{1}$$

where Ω denotes a neighbourhood of the current pixel, $\boldsymbol{c}$ and scalar k are defined by Eq. 2, $f_x(\cdot)$, $f_y(\cdot)$, $f_z(\cdot)$, and $f_t(\cdot)$ are spatial and temporal derivatives of $f(\cdot)$.

$$\begin{aligned} k &= f_t - f + x f_x + y f_y + z f_z \\ \boldsymbol{c} &= (x f_x, y f_x, z f_x, x f_y, y f_y, y f_y, x f_z, y f_z, z f_z, f_x, f_y, f_z, -f, -1)^T \end{aligned} \tag{2}$$

A smoothness constraint is then imposed on the model parameters $\boldsymbol{m}$ and the error function is augmented by this, which penalises solutions proportional to the local change in each parameter across a small spatial neighbourhood. The error function, defined in such a way, allows for a locally smooth, but globally non-rigid transformation. Minimisation of the error function was done through differentiating, setting the result to zero and solving for $\boldsymbol{m}$.

The entire procedure is built upon a differential multiscale framework [10], that permits the capture of both large- and small-scale transformations.

3.1 Euclidean-Lagrangian Extension

Let U^{AB} denote a transformation between target A and source B obtained with the algorithm described above. For a sequence of volumes $I_1, ..., I_N$, we can derive $U^{I_1 I_2}, U^{I_1 I_3}, ..., U^{I_1 I_N}$. Let $\Im_k$, $k = 1..N$ denote the output: $\Im_k = U^{I_1 I_k}[I_k] \approx I_1$.

Geometric differences between pre- and post-contrast image might not be significant, however contrast and brightness variations, especially in the datasets acquired from the patients severely affected by RA, are dramatic. Thus, alignment of the post-contrast images to the first one of a dynamic series might not be accurate.

To minimise the registration error the transformation could be performed in an incremental rather than pair-wise fashion (a.k.a. Euclidian approach). However, if the alignment between the volumes at the beginning was not accurate, the error would further propagate. To overcome this, the output of this sequential transformation is used as an initial solution for the basic registration algorithm. Such an approach is often referred to as Lagrangian.

So, for a DCE-MRI dataset, we firstly determine transform between neighbouring volumes, where the contrast and brightness variations are less significant:

$$V^{I_k} = U^{I_1 I_2} \otimes ... \otimes U^{I_{k-2} I_{k-1}} \otimes U^{I_{k-1} I_k} \tag{3}$$

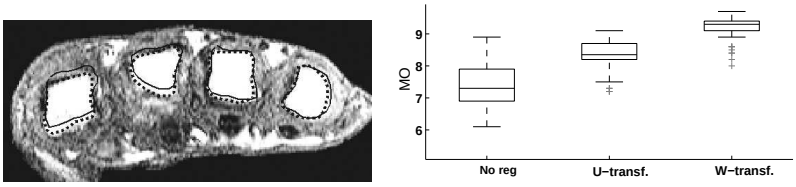

Fig. 1. Left: Bone interiors outlined in source and superimposed on target before (solid) and after (dashed) registration with W-transformation. Right: MO between bone regions in source and target in 200 images before registration, and after images were aligned with the registration with basic U- and proposed W-transformations.

This transformation applied to the k^{th} volume yields the volume J_k, $J_k = V^{I_k}[I_k] \approx I_1$. However, if the alignment of the first volumes was not perfect, registration error would propagate when registering volumes from later in the study. To compensate for this possible error, a sequence of volumes registered in the sequential manner $\{J_k\}_{k=1\ldots N}$ is taken as an initial solution for the basic registration algorithm.

Then, the final transform is defined as $W^{I_k} = U^{I_1 J_k} \otimes V^{I_k}$, and being applied to the k^{th} volume yields the volume L_k, $L_k = W^{I_k}[I_k]$. With this approach a DCE-MRI study is considered as a whole, which permits reduction of the transformation error and allows compensation for contrast and brightness variations between the images.

4 Discussion

To evaluate registration with U-, V-, and W-transformations, we measured mutual overlap (MO) [11] between manually outlined rigid bone interiors in 200 source and target images before and after the registration. Fig. 1 illustrates positions of bone interiors before and after registration in a sample image (left). True bone interiors outlined in the target are shown in white. Contours of the bone interiors from the source image before (solid line) and after (dashed) registration were superimposed on the target. MO here has increased from 0.76 to 0.92. The same experiment was performed on 200 images and the results are shown in Fig. 1 (right).

MO before registration was on average 0.74 with the minimum at 0.53 and standard deviation, $\sigma = 0.07$. After registration with the U-transformation, it became 0.8 with $\sigma = 0.06$; after registration with the V-transformation – 0.81 with $\sigma = 0.04$. Finally, when the W-transformation was applied, the mutual overlap became on average 0.92 with $\sigma = 0.03$.

The appearance of the images before and after registration with the proposed transformation is visibly different and medical observers' judgement was positive. The algorithm has not failed on any of the images. Registration permits reduction of the noise artefacts and significant improvement in the location of

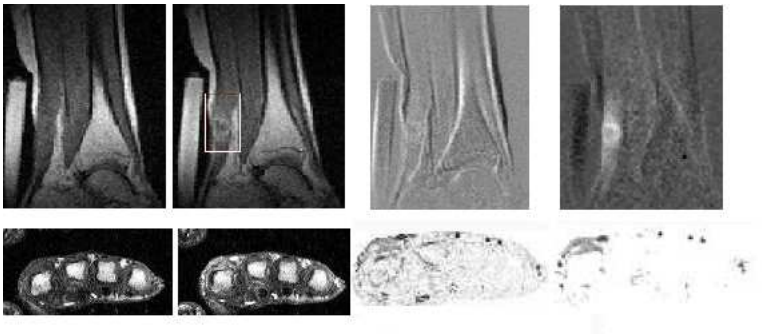

Fig. 2. Pre-contrast (a), post-contrast (b) images of the MCPJs (bottom) and tendon (top) and subtractions between pre- and post- contrast images before (c) and after (d) registration. After registration, artefacts have been reduced; shape and location of the inflamed areas are clearer.

the blood vessels, bone interiors, skin, but most importantly synovial tissue. This is especially prominent on the data acquired with the low-field scanner (Fig. 2, top), where the signal to noise ratio is significantly lower and acquisition times are longer. Fig. 2 illustrates pre- and post-contrast images and their subtraction before and after registration.

To evaluate the improvement in visual appearance, we subtracted source before and after registration from the target and estimated the mean square errors (MSE) on intensity values of subtracted images.

Ideally, in the absence of patient motion and contrast agent MSE between the registered images should be zero. However, due to the effect of the contrast agent, MSE is always greater than zero, reflecting the magnitude of the enhancement. Figures 3 illustrates MSE computed before and after the registration with various transformations applied to 100 images.

The shape of the MSE graphs corresponds to the expected change in the intensity. The major variations of the intensity occur at the wash-in and wash-out phases. At the baseline and plateau phases (1-3 and 7-16 time instants, respectively), where no significant intensity changes are expected, reduction in MSE can be attributed mostly to the effect of the registration. This experiment demonstrate that on average for the high-field data MSE has decreased from 0.35 to 0.2 and for low-field data from 0.25 to 0.08.

4.1 Estimation of enhancement curves

Normally, to perform quantitative analysis of DCE-MRI data, a clinical expert extracts from a small ROI signal intensity vs. time curves. Parameters describing their shape (maximum of intensity and a slope) are then extracted. Curves corresponding to the inflamed synovial tissue exhibit steep wash-in, high maximum

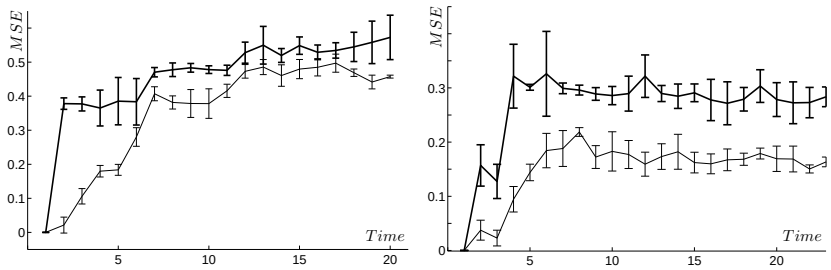

Fig. 3. MSE between 100 target and source images acquired with the high-field (left) and low-field (right) scanners and aligned with the registration with U-(bold) and W-(thin) transformations. The length of the error bars is 1.96σ. Time - number of frames per acquisition.

intensity values, and a wash-out phase. Curves corresponding to tissue which is not affected by RA normally exhibit no enhancement.

Patient motion can change the shape of the enhancement curves. Fig. 4 illustrates signal intensity vs. time curves before (left) and after (right) the registration. A comparison of these two sets suggests that significant movement occurred between 5^{th} and 10^{th} time instants. Evidently, enhancement curves extracted from the registered images show much less variation during the wash-in and equilibrium phases.

The bold black curve (the mean) is the one used by the radiologist to evaluate the nature of the enhancement. Without registration, the curve shows continues increase and no wash-out phase, despite the fact that enhancement of the inflamed synovium is expected to peak around the 15^{th} time instance. After registration, the behaviour of the enhancement curves corresponds much better to the nature of the enhancement: with more pronounced wash-in and wash-out phases, evaluation of the inflammation can be performed more accurately. This experiment illustrates that registration significantly improves the accuracy of the estimation.

Fig. 5 illustrates parametric maps of maximum enhancement (ME), computed with the automated quantitative approach [3], superimposed on low-field post-contrast image of the wrist (top) and MCPJs (bottom), extracted from active RA patient and healthy control, respectively. In the top row, it is expected that synovial tissues and erosions will exhibit high ME (yellow-white colours), intermediately active tissues will be coloured in dark red, and non-enhancing tissue have no colour. Before the registration (mid) the most significant enhancement corresponds to skin area; the joint with an erosion in the center is shown in darker red colours. After registration, a quantitative map of ME reflects expected activation events (pixels within an erosion are in white-yellow). In the bottom row, the ME map for a healthy control should only show enhancement within the blood vessels. Before registration, we observe some activation around

the joints, after the registration, the inflammation map corresponds precisely to clinical expectation. This demonstrates that the algorithm allows elimination of the artifactual enhancement.

5 Conclusion

The paper discussed registration algorithm for alignment of non-rigid multi-slice DCE-MRI data, which accounts for significant variations in contrast and brightness that occur in the post-contrast volumes. The approach was demonstrated on data acquired from active RA patients using low and high field scanners. Enhancement curves extracted from the registered images demonstrate less variability and more distinguished wash-in and wash-out phases. The registration algorithm has significant impact on the accuracy of quantitative analysis techniques and allows for significant reduction of the artefactual enhancement. This contributes to the data fidelity for diagnosis of RA.

The scheme presented here is yet to be tested with other similarity measures such as local normalised cross-correlation, correlation ratio or mutual information [7] and in application to other DCE-MRI studies. Our preliminary experience suggests that it is acceptable for a wider application.

References

1. Silman, A.J., Pearson, J.E.: Epidemiology and genetics of rheumatoid arthritis. Journal of Arthritis Research and Therapy **4**(3) (2002) S265–S272
2. Tofts, P.S.: Modelling tracer kinetics in dynamic Gd-DTPA MR imaging. Journal of Magnetic Resonance Imaging **7**(1) (1997) 91–101
3. Kubassova, O., Boesen, M., Boyle, R.D., Cimmino, M.A., Jensen, K.E., Bliddal, H., Radjenovic, A.: Fast and robust analysis of dynamic contrast enhanced MRI datasets. In: MICCAI. Volume 2. (2007) 261–269
4. Cimmino, M.A., Innocenti, S., Livrone, F., Magnaguagno, F., Silvesti, E., Garlaschi, G.: Dynamic gadolinium-enhanced MRI of the wrist in patients with rheumatoid arthritis. Arthritis and Rheumatism **48**(5) (2003) 674–680

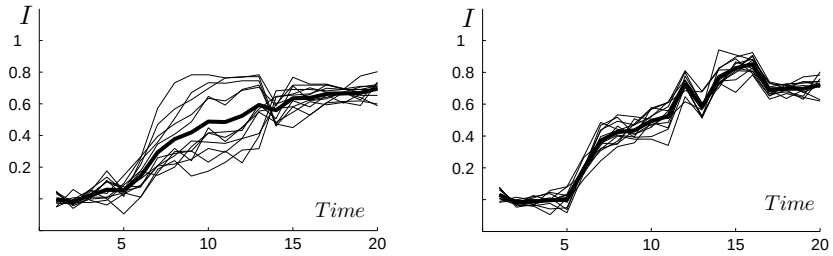

Fig. 4. Enhancement curves extracted from region-of-interest before (left) and after (right) registration. I - normalised signal intensity. $Time$ - a number of frames per acquisition.

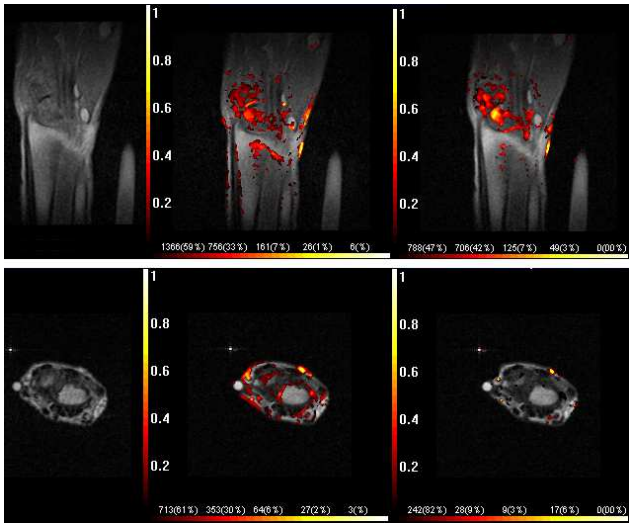

Fig. 5. From the left: post contrast image, map of ME before and after registration. Top: evaluation of active patient with RA in wrist. After the registration, erosion is highlighted white-yellow, which indicates the highest activity and corresponds to clinical expectation. Bottom: evaluation of healthy control. After the registration, a number of colour pixels is reduced and as expected, no enhancement is present near the joints. Maps are produced by DYNAMIKA^{TM}, www.image-analysis.org

5. Zou, C., Jiang, A., Buff, B.L., Mahon, T.G., Wong, T.Z.: Automatic motion correction for breasts MR imaging. Radiology **198**(3) (1996) 903–906
6. Kumar, R., Hanna, K., Asmuth, J.C., Bergen, J.R., Hulka, C., Kopans, D.B., Weisskoff, R., Moore, R.: Detecting lesions in magnetic resonance breast scans. In: Proceedings of SPIE 24th AIPR Workshop on Tools and Techniques for Modeling and Simulation. (1996) 181–190
7. Crum, W.R., Tanner, C., Hawkes, D.J.: Anisotropic multi-scale fluid registration: evaluation in magnetic resonance breast imaging. Electronic Journal on Physics in Medicine and Biology **50**(21) (2005) 5153–5174
8. Froh, M.S., Barber, D.C., Brock, K.K., Plewes, D.B., Martel, A.L.: Piecewise-quadrilateral registration by optical flow – applications in contrast-enhanced MR imaging of the breast. In: Proceedings of International Conference on Medical Image Computing and Computer-Assisted Intervention. Volume 2. (2006) 686–693
9. Periaswamy, S., Farid, H.: Medical image registration with partial data. Medical Image Analysis **10**(3) (2006) 452–464
10. Nestares, O., Heeger, D.J.: Robust multiresolution alignment of MRI brain volumes. Journal of Magnetic Resonance in Medicine **43**(5) (2000) 705–715
11. Dice, L.R.: Measures of the amount of ecologic association between species. Journal of Ecology **26**(3) (1945) 297–302